processes

MDPI

Article

Experimental and Simulation Research on Heat Pipe Thermal Management System Coupled with Battery Thermo-Electric Model

Ying Xu [1], Zhiqiang Wang [1,2], Zhaoqing Ke [1], Bozhen Lai [1], Ying Zhang [1,*] and Xingyuan Huang [1,*]

[1] School of Advanced Manufacturing, Nanchang University, Nanchang 330031, China
[2] School of Mechanical and Vehicle Engineering, Nanchang Institute of Science and Technology, Nanchang 330108, China
* Correspondence: yzhan@ncu.edu.cn (Y.Z.); xyhuang@ncu.edu.cn (X.H.)

Abstract: The lithium-ion battery is widely used in the power system of pure electric vehicles and hybrid electric vehicles due to its high energy density. However, the chemical and electrochemical reactions generate a lot of heat. If the heat is not transferred through some refrigeration methods in time, it will lead to a rapid rise in the temperature of the battery. In this paper, an electric–thermal coupling model of a cylindrical Panasonic 21700 battery was proposed by using offline parameter identification method. Based on this model, a battery thermal management system using a heat pipe was established. The experimental results show that the model can simulate the actual performance of battery well. When the ambient temperature is 25 °C, the battery parameters change little and battery performance is better. The heat pipe battery thermal management system performs better than the non-heat pipe battery system in the discharge process, and can control the battery temperature well at low and high temperatures. Changing the refrigerant temperature can achieve a better thermal management effect under suitable ambient temperature conditions.

Keywords: offline parameter identification; heat pipe; thermal management system; electrochemical energy; numerical simulation

Citation: Xu, Y.; Wang, Z.; Ke, Z.; Lai, B.; Zhang, Y.; Huang, X. Experimental and Simulation Research on Heat Pipe Thermal Management System Coupled with Battery Thermo-Electric Model. *Processes* **2023**, *11*, 1204. https://doi.org/10.3390/pr11041204

Academic Editor: Gang Wang

Received: 18 March 2023
Revised: 7 April 2023
Accepted: 11 April 2023
Published: 13 April 2023

1. Introduction

Lithium-ion batteries boast an energy density that is four to five times greater than that of lead-acid batteries, making them a popular choice for power systems in pure electric and hybrid vehicles. These batteries are typically arranged in series and parallel configurations to provide the necessary energy for vehicle operation. However, the charging and discharging process of the battery pack can generate significant amounts of heat through chemical and electrochemical reactions. Without proper cooling methods, this heat can accumulate within the battery pack, causing a rapid increase in temperature that can be detrimental to the battery's performance. Excessively high battery temperatures can have detrimental effects on battery performance, hasten battery aging, and even trigger thermal runaway, potentially leading to fires in extreme cases. To regulate temperature during the charging and discharging of batteries, numerous scholars have explored the use of lithium-ion batteries in electric vehicles, with the electric–thermal coupling model of lithium-ion batteries serving as a crucial tool for investigating battery pack applications in electric vehicles [1]. Currently, common modeling methods for lithium-ion batteries include partial differential equation thermal models, linear parametric models, finite element models, electrochemical models, and equivalent circuit models [2]. Hallaj et al. [1] put forward a straightforward one-dimensional mathematical model to simulate the heat production rate of cylindrical SONY US18650 batteries, and validated the model's accuracy with experimental data. Smyshlyaev et al. [3] developed a two-dimensional partial differential equation thermal dynamics model for lithium-ion batteries. This model significantly

reduces the computation time compared to the computational fluid dynamics (CFD) model, while maintaining high accuracy in calculations. Hu et al. [4] proposed a space algorithm-based line variable parameter (LVP) identification method that simplifies the traditional LVP model to some extent. Mi et al. [5] utilized the finite element method to establish a two-dimensional static finite element model for a lithium-ion battery pack (containing 48 cells), assuming that the cell was a constant heat source with a heat generation rate of 2.71 W. The model simulated the maximum and minimum temperature rise and temperature gradient of the battery under natural convection conditions (ambient temperature was 25 °C), and the error between simulation results and test data was within 3%. Shrimali et al. [6] established the electrochemical model—Newman Pseudo-Two-Dimensional model—for commercial 18,650 batteries based on the theory of porous electrode and the principle of concentrated solution, and applied this model to three 18,650 batteries with different anode and cathode materials. The temperature distribution and voltage values of the three batteries were compared and analyzed across three discharge rates and tropical ambient temperatures. However, it should be noted that this study lacks verification of model accuracy. Oehler [7] integrated the electrochemical model with the extended Kalman filter algorithm to create a more practical electrochemical model for online applications, which overcomes the complexity of traditional electrochemical models. However, experimental validation is still required. Damay et al. [2] examined the thermal–thermogenesis coupling model of large lithium-ion batteries using the lumped parameter method, and confirmed the model's reliability through cyclic discharge experiments. The simplified computation of the model makes it ideal for embedded applications.

Lin et al. [8] developed a battery electronic model and a thermionic model, which were subsequently integrated into a battery electric–thermal coupling model. This integration was achieved by considering heat production, temperature, and the impact of temperature on the electrical model's parameters. The electric model's parameters were calculated using a combination of parameter identification and the least square method under isothermal conditions, while the thermal control model's parameters were identified using a combination of experimental data and the least squares method. The model was validated using impedance spectrum method and cyclic test data. However, the validation results revealed that the model did not account for the hysteresis phenomenon, resulting in significant errors in the identified parameters at high and low frequencies.

Based on the studies conducted by numerous scholars, the life cycle and charge–discharge performance of batteries are significantly impacted by both high and low temperatures, as well as temperature inhomogeneity within the battery module [9–13]. Some scholars have found that in the absence of a reasonable heat management system, the temperature of battery charging and discharging can be higher than 50 °C, or even reach the temperature of thermal runaway [14–17]. Therefore, numerous scholars have conducted extensive research on battery thermal management schemes based on the battery model. These thermal management strategies primarily comprise air cooling, liquid cooling, phase change material cooling, heat pipe cooling, and thermo-electric cooling. Air cooling reduces battery temperature mainly by circulating cold air between battery modules. Based on energy consumption, air cooling can be categorized into passive air cooling and active air cooling [15]. Active air cooling mainly employs air pre-cooled by air conditioning to cool the battery, while passive air cooling directly utilizes ambient air [16]. The air cooling system has a simple structure and has minimal impact on battery energy density, but its cooling efficiency is low. Considering the suboptimal cooling efficiency of the air cooling system, the researchers endeavored to enhance it by optimizing the air duct geometry, modifying the unit layout gap, and refining the airflow flow path, among other techniques [17–23].

As the air cooling method proved to be ineffective for cooling high-power batteries, researchers shifted their focus towards alternative cooling methods [24]. Li et al. [25] designed a microchannel cooling system using CFD numerical simulation and multi-objective genetic algorithm optimization of different design variables to obtain the optimal system design. The results showed that the thermal management efficiency and battery life

cycle of the system were significantly improved, while the weight and cost of the system were reduced. Lan et al. [26] improved the heat transfer efficiency of lithium-ion batteries by wrapping aluminum flat tubes around square batteries, and setting small channels in the tubes as cooling fluid channels. The study showed that microchannel aluminum tubes can effectively improve the thermal conductivity of lithium-ion batteries, reduce battery temperature, and, thus, improve battery performance and life cycle. This study provides a new idea and method for the thermal management of lithium-ion batteries. Kairat et al. [27] used a baffle plate and flow guide vanes in the battery cooling system, and the study showed that these technologies can significantly improve the cooling efficiency of the battery module and reduce the temperature unevenness of the battery module. In addition, the design and position of the baffle plate and flow guide vanes have an important impact on the cooling effect. Therefore, these factors should be considered in the design and manufacture of battery modules to improve cooling efficiency and battery life cycle. Qian et al. [28] studied the use of microchannel cooling technology to improve the thermal performance of lithium-ion battery thermal management systems and the impact of microchannel cooling system design parameters on battery thermal performance, and proposed an optimized design scheme. The study showed that using microchannel cooling can significantly improve the thermal transfer efficiency of the battery and reduce the battery temperature.

Using phase change material (PCM) between cells can overcome the problem of large temperature difference between cells [29,30]. Wilke et al. [31] demonstrated that incorporating PCM between battery cells can effectively mitigate temperature rise and temperature variation within battery modules. However, the low thermal conductivity of PCM materials has limited their application in battery thermal management systems. Consequently, researchers have conducted extensive investigations to enhance the thermal conductivity of PCM materials, including the addition of carbon nanopowders with specific sizes [32], utilization of nanoparticles [33,34], incorporation of metal layers between PCM materials and battery surfaces, and utilization of porous materials. Despite the significant improvement in thermal conductivity achieved by these methods, there are still several challenges in the practical application of PCM. As a result, the application of PCM in electric vehicles remains a challenging task at present [35].

Furthermore, a plethora of experiments and simulations have been conducted on thermo-electric cooling (TEC) [36–38], heat pipe cooling (HPC) [39–46], and the integration of multiple cooling techniques. Table 1 provides a comprehensive overview of other pertinent investigations on power battery thermal management systems.

Although numerous scholars have conducted research on the battery model and thermal management system, and have arrived at effective conclusions, few studies have verified the consistency between the battery model and experimental research under varying working conditions. Furthermore, there is a dearth of research on heat pipe thermal management systems that are based on battery electrothermal coupling models. This is primarily due to the complexity of battery model parameters under different working conditions.

In this paper, a significant number of battery discharging experiments were conducted under various conditions using the offline parameter identification method. Based on the extensive experimental data, the parameters of the established electric–thermal lumped lithium-ion battery model were identified, enabling the creation of a more precise electric–thermal model of the lithium-ion battery. Subsequently, the heat transfer and flow model of the heat pipe were established, and the electric heating model of the lithium-ion battery was coupled with the heat transfer flow model of the heat pipe.

Table 1. Summary of other cell thermal management studies [47].

Cooling Method	Research Methodology	Heat Source	Cold Source	Author
TEC + Liquid cooling	Experimental Simulation	Cell	Water	Lyu [37]
TEC-based cooling	Experimental	Heater	Water	Lyu [38]
TEC + PCM	Simulation	Battery	TEE	Liao [39]
Tubular HPC	Experimental	Electric heater	Water-cooled channel	Liang et al. [40]
Tube HPC	Experimental Simulation	Electric heater	Forced convection (with finned array)	Yuan et al. [41]
L-shaped flat HPC	Experimental	Cell	Forced convection	Wu et al. [42]
HPC with cylindrical fins	Experimental	Heating rod	-Air cooling -PCM coupled heat pipe	Zhao et al. [43]
HPC	Experimental Simulation	A polyimide heater	Natural convection	Yamada et al. [44]
Flat HPC	Experimental	Electric heater	Natural and forced convection	Tran et al. [45]
HPC	Experimental	Analog cell tank	Liquid tank	Wang et al. [46]
HPC	Experimental	Electric heater	-Adiabatic -Forced Convection	Tran et al. [48]

2. Experiment Setup

In this study, we utilized a battery tester named CN-CD30V10 to charge and discharge a Panasonic 21,700 lithium-ion battery at varying temperatures. Through the collection of experimental data at different temperatures, we were able to determine the offline parameters of the lithium-ion electric–thermal coupling model. The electrochemical and related geometric parameters of the Panasonic 21,700 lithium-ion battery can be found in Table 2.

Table 2. Electrochemical and geometric parameters of Panasonic 21,700 lithium-ion battery.

Battery Specification	Value	Geometrical Parameter	Value	Chemical Composition	Value
Type	21,700 A	Diameter (m)	0.021	Positive electrode	Lithium cobaltate ternary
Rated Capacity	4800 mAh	Mass (kg)	0.069	Negative electrode	Silicon-based graphite
Nominal Voltage	3.7 V	Height (m)	0.07	Electrolyte	EC:DMC:EMC
Charge Cut-off Voltage	4.2 V	-	-	Diaphragm	Polyethylene coating ceramics
Discharge Cut-off Voltage	2.5 V	-	-	-	-

To identify parameters for the battery electric model, we utilized intermittent constant-current potentiometric titration to determine the V_{ocv} and C_{bat} of the battery. This allowed us to acquire the state of charge (SOC)-open circuit voltage (OCV) curve and battery capacity under varying working conditions. The battery was tested in a thermal controlled chamber with a controllable temperature range of −5 °C to 65 °C, meeting the temperature requirements outlined in this study.

For the battery thermal model parameters identification, we employed the method of constant-current discharge of the battery, and used a temperature sensor to record the transient temperature change of the battery during the discharge process. The temperature sensor was placed at the position of the battery pole, and the measured temperature of the

battery pole was substituted for the internal temperature of the battery. We used the pole temperature of the battery to identify the parameters of the battery thermal model because the axial heat conduction coefficient of the battery was large, and the pole temperature was closer to the core temperature of the battery than the temperature of other positions on the battery surface. We carried out the offline parameter identification of battery thermal model parameters by using 2C discharge rate at different temperatures.

3. Model Development

3.1. Cell Model

In this section, we establish an electric–thermal coupling model for lithium-ion batteries. To simulate the electrical characteristics of the battery, we employ an equivalent circuit electrical model.

3.1.1. Electric Model of Lithium-Ion Battery

The electrical model presented in this paper utilizes the equivalent circuit model, an empirical model that characterizes the external current–voltage characteristics of the battery without delving into the specific electrochemical processes occurring within it. The schematic diagram of the equivalent circuit model is depicted in Figure 1.

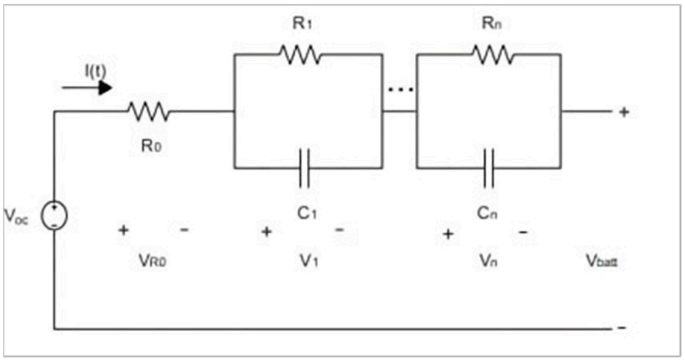

Figure 1. Equivalent circuit model.

The terminal voltage of the battery consists of three parts [8]:

$$V_T = V_{OCV} - IR_S - \sum_{i=1}^{n} V_{RC,i}. \quad (1)$$

In the formula, V_T is the equivalent circuit terminal voltage; V_{OCV} is open circuit voltage, generally related to temperature and SOC; IR_S is the voltage drop of the series battery resistance; and $\sum_{i=1}^{n} V_{RC,i}$ is the voltage drop of RC link.

Coulomb counting method is used to calculate SOC [8]:

$$\frac{dSOC}{dt} = -\frac{1}{C_{bat}} I, \quad (2)$$

where C_{bat} represents the battery's capacity, while I denotes the excitation current. $V^{RC,i}$ is used to describe the voltage change during the transient process of the battery:

$$\frac{dV_{RC,i}}{dt} = -\frac{1}{R_i C_i} V_{RC,i} + \frac{1}{C_i} I, \quad (3)$$

where R_i, C_i represent the resistance and capacitance of RC link, respectively; they are related to SOC, temperature, and excitation current, and the value needs to be determined according to parameter identification.

3.1.2. Battery Thermal Model

The battery thermal model presented in this paper is based on several fundamental assumptions:

(1) It is assumed that the battery is a uniformly hot mass.
(2) The cell pole lug temperature is assumed to replace the cell center temperature.
(3) The cylindrical cell is assumed to be radially and transversely anisotropic, but with uniform thermal conductivity.

To establish the battery thermal physical model, Matlab/Simscape R2022b was utilized. The model leveraged the similarity of dynamic characteristic equations of different physical systems and identified the corresponding relationship between thermal characteristic parameters and electrical characteristic parameters, as illustrated in Table 3. The thermal characteristic was then described as an equivalent electrical characteristic grid.

Table 3. Relationship between battery thermal characteristics and electrical characteristic grid parameters.

Hot Domains	Electric Domains
Temperature	Voltage
Heating Power	Current Source
Heat Capacity	Capacity
Heat Resistance	Resistance

3.1.3. Battery Heat Generation Model

The total heat production of the battery can be divided into four parts:

(1) electric loss heat production (irreversible heat);
(2) entropy heat (reversible heat);
(3) side reaction heat;
(4) mixing heat.

The mixed heat in the battery is linked to the concentration gradient of lithium ions within. When a concentration gradient is established, the mixed heat is negative. However, when the concentration gradient dissipates, the mixed heat becomes positive, resulting in a total mixed heat of zero. The heat produced by side reactions primarily pertains to battery aging, which is not addressed in this article, hence the heat generated by side reactions is disregarded. Therefore, the total heat generated by the battery, as discussed in this article, is the combination of Joule heat and entropy heat [2].

The Bernardi equation was used to calculate the overall heat generation of the battery:

$$\dot{Q} = \dot{Q}_{elec} + \dot{Q}_{\Delta S}, \tag{4}$$

where the total heat generated by a battery is referred to as $\dot{Q}$, $\dot{Q}_{elec}$ denotes the heat produced by electric loss, and $\dot{Q}_{\Delta S}$ represents the entropy heat:

$$\dot{Q}_{\Delta S} = I_{cell} T_{in} \frac{\partial U_{oc}}{\partial T}, \tag{5}$$

where $\dot{Q}_{\Delta S}$ denotes entropy heat, I_{cell} represents battery excitation current, and T_{in} is battery internal temperature. In this paper, the electrode ear temperature measured experimentally is utilized to replace the internal cell temperature. $\frac{\partial U_{OC}}{\partial T}$ represents the temperature coefficient of open circuit voltage, which can be calculated from the experimental data table:

$$\dot{Q}_{elec} = I_{cell} \times \Delta U = I_{cell} \times (U_{cell} - U_{OC}), \tag{6}$$

where U_{cell} denotes the cell real-time voltage, and U_{OC} represents the battery open-circuit voltage.

3.1.4. Cell Heat Transfer Model

As the cell utilized in the experiment is cylindrical in shape, the heat transfer model of the cell takes the form of cylindrical coordinates.

Battery thermal conductivity calculation model is as follows:

$$\rho c \frac{\partial T}{\partial t} = \frac{1}{r}\frac{\partial}{\partial r}(\lambda_r r \frac{\partial T}{\partial r}) + \frac{\partial}{\partial z}(\lambda_z \frac{\partial T}{\partial z}) + q, \tag{7}$$

where ρ represents battery density, c denotes specific heat capacity, λ_r denotes radial thermal conductivity, λ_z is axial thermal conductivity, and q is battery heat flux density.

Battery heat transfer calculation model consists of two equations:

$$q_{f1} = h_1(T - T_{amb}), \tag{8}$$

$$q_{f2} = h_2(T - T_{cool}), \tag{9}$$

where q_{f1} represents the convective heat transfer density between the cell and world, T represents the battery temperature, T_{amb} represents the ambient temperature, h_1 represents the convective heat transfer coefficient between the battery and the heat pipe, q_{f2} represents the convective heat transfer density between the battery and the heat pipe, h_2 represents the convective heat transfer coefficient between the cell and heat pipe, and T_{cool} represents the refrigerant temperature of the condensing section of the heat pipe.

3.2. Heat Pipe Model

This paper focuses on the investigation of thermal management strategy for horizontal heat pipe systems. The heat pipe comprises an evaporator section at one end, a condenser section at the other end, and an insulated section in the middle. When the battery temperature is high, the outer surface of the battery gets heated, which, in turn, heats up the evaporator section of the heat pipe, leading to the evaporation of the liquid in the wick. The vapor then moves to the condenser section, where it releases heat and condenses into liquid due to a slight pressure difference. The liquid then flows back to the evaporator section through capillary action via a porous material, and the process repeats. The condenser section is cooled by a heat exchanger. Conversely, when the battery temperature is low, the heat exchanger provides heat to the evaporator section of the heat pipe, causing the liquid in the wick to evaporate. The vapor then moves to the condenser section, where it releases heat to warm up the battery. Figure 2 illustrates a thermal management model for a single battery that utilizes a heat pipe system.

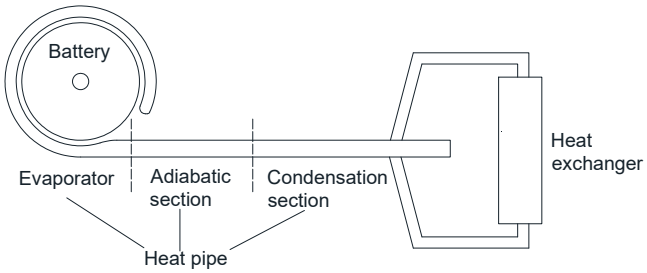

Figure 2. A thermal management model for a single battery utilizing heat pipe technology.

The heat pipe model is a fluid model that undergoes phase change. The interior of the heat pipe comprises a liquid-phase region, a gas–liquid mixed-phase region, and a gas-phase region. To track these three regions, a boundary tracking model is employed. The proportion of space that each region occupies in the system is referred to as the regional length fraction,

$$Q_F = Q_{F,L} + Q_{F,V} + Q_{F,M}, \tag{10}$$

where Q_F represents the overall heat transfer; $Q_{F,L}$ denotes the heat transfer occurring between the liquid phase region and the tube wall; $Q_{F,V}$ refers to the heat transfer between the gas phase region and the tube wall; and $Q_{F,M}$ represents the heat transfer taking place between the mixed phase region and the tube wall. The three components are calculated as follows:

$$Q_{F,L} = \dot{m}_Q c_{p,L}[T_{W,L} - \min(T_L, T_S)[1 - \exp(-\frac{z_L S_W \alpha_L}{\dot{m}_Q c_{p,L}})], \tag{11}$$

$$Q_{F,M} = (T_H - T_{Sat}) z_M S_W \alpha_M, \tag{12}$$

$$Q_{F,V} = \dot{m}_Q c_{p,V}[T_{W,V} - \min(T_L - T_{Sat})[1 - \exp(-\frac{z_V S_W \alpha_V}{\dot{m}_Q c_{p,V}})], \tag{13}$$

where $\dot{m}_Q$ represents the mass flow rate of the fluid flowing through the tube; $c_{p,L}$ and $c_{p,V}$ denote the specific heat capacity of the liquid and gas phases, respectively; T_L is the liquid inlet temperature; T_H is the external temperature; T_S represents the saturation temperature of the fluid; $T_{W,L}$ is the temperature of the wall around the liquid region; $T_{W,V}$ is the temperature of the wall around the gas phase region; z_L, z_M, z_V represent the length fraction of the liquid phase, the mixed phase and the gas phase, respectively; α_L, α_M, α_V represent the convective heat transfer coefficient between the liquid-phase, the mixed-phase, the gas-phase region and the pipe wall, respectively; and S_W represents the surface area of the pipe. Heat transfer between the heat pipe and its surroundings are calculated by

$$Q_H = Q_{H,L} + Q_{H,V} + Q_{H,M}, \tag{14}$$

$$Q_{H,zone} = (T_H - T_W)_z S_W \alpha_E, \tag{15}$$

where Q_H is the total heat exchange volume between the surface of the heat pipe and the external environment, and $Q_{H,zone}$ is the heat exchange volume between the wall surface of each region and the outside world.

The Continuity Equation is represented by

$$\frac{dM}{dt} = \dot{m}_A + \dot{m}_B, \tag{16}$$

$$\frac{dM}{dt} = [(\frac{d\rho}{dp})_u \frac{dp}{dt} + (\frac{d\rho}{du})_p \frac{du_{out}}{dt} + \rho_L \frac{dz_L}{dt} + \rho_M \frac{dz_M}{dt} + \rho_V \frac{dz_V}{dt}]V, \tag{17}$$

where M represents the total mass of the fluid in the pipe, ρ represents the fluid density, p represents the pressure, u represents the specific internal energy, and u_{out} denotes the specific internal energy of the fluid at the pipe's exit.

The Momentum Equation is represented by

$$p_A - p_I = (\frac{1}{\rho_I} - \frac{1}{\rho_A^*})(\frac{\dot{m}_A}{S})^2 + \frac{\lambda \mu \dot{m}_A}{2\rho_I D_H^2 S}(\frac{L + L_{Add}}{2}), \tag{18}$$

$$\mu = \mu_L z_L + \mu_M z_M + \mu_V z_V, \tag{19}$$

$$p_B - p_I = (\frac{1}{\rho_I} - \frac{1}{\rho_B^*})(\frac{\dot{m}_B}{S})^2 + \frac{\lambda \mu \dot{m}_B}{2\rho_I D_H^2 S}(\frac{L + L_{Add}}{2}), \tag{20}$$

where p_A and p_B are the pressure of ports A and B, respectively, p_I is the pressure of internal nodes, and μ is the average dynamic viscosity.

The Energy Conservation Equation is represented by

$$M\frac{du_{out}}{dt}(\dot{m}_A + \dot{m}_B)u_{out} = \varphi_A + \varphi_B + \varphi_F, \tag{21}$$

where φ_A and φ_B are the energy flow rates of ports A and B, respectively.

4. Offline Parameter Identification

4.1. Experimental Results and Analysis

The experiment has been divided into three parts. Firstly, the SOC–OCV curve and battery capacity were measured under different working conditions using intermittent constant-current potentiometric titration. Secondly, the experimental conditions were changed, including ambient temperature and discharge rate, and the change in battery terminal voltage was recorded. Lastly, the experimental conditions were changed again, and the transient temperature of the battery was recorded.

It should be noted that the SOC–OCV curve and actual battery capacity are not only affected by ambient temperature, but also by the discharge current of the cell. Therefore, this experiment measured the SOC–OCV curve of the cell at various ambient temperatures and measured the actual capacity of the cell at various ambient temperatures with varying discharge rates. The results of the SOC–OCV curve experiment are presented in Figure 3, while the results of the actual battery capacity experiment are shown in Table 4.

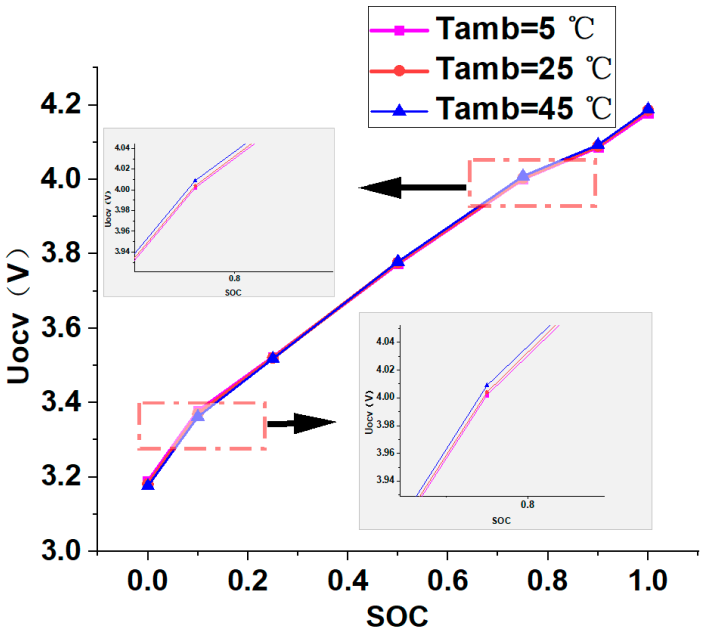

Figure 3. Battery SOC–OCV curve.

Table 4. Actual battery capacity.

Discharge Rate \ Ambient Temp	5 °C	25 °C	45 °C
1C	4.3 Ah	4.46 Ah	4.56 Ah
1.5C	4.55 Ah	4.64 Ah	4.78 Ah
2C	4.54 Ah	4.61 Ah	4.75 Ah

Battery Transient Terminal Voltage and Temperature Changes under Different Working Conditions

To aid in identifying the electric and thermal model parameters of the battery, the actual terminal voltage and temperature of the battery pole were measured during a 2C discharge rate, with consideration given to the discharge depth. As the average temperature and terminal voltage of the battery are influenced by the ambient temperature, the experiment also involved adjusting the ambient temperature using the thermal controlled chamber's temperature regulation function. This allowed for the determination of how the terminal

voltage and pole temperature of the cell change with discharge depth under varying ambient temperatures.

Figure 4 illustrates the changes in transient terminal voltage and pole temperature of the cell as discharge depth varies under different ambient temperatures and a 2C discharge rate.

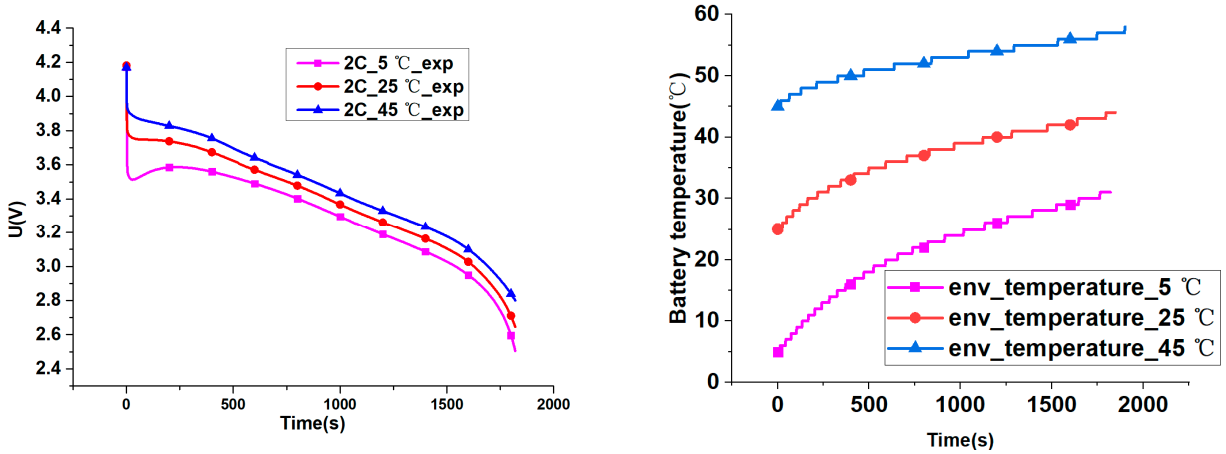

(**a**) (**b**)

Figure 4. (**a**) Battery transient terminal voltage varies with discharge depth at different ambient temperatures; (**b**) Electrode temperature changes with discharge depth at different ambient temperatures.

Based on Figure 4a, the battery terminal voltage exhibits a consistent trend across different ambient temperatures. This indicates that the voltage drops abruptly at the onset of discharge, primarily due to the presence of ohmic impedance, and then gradually decreases until the end of discharge. At the end of discharge, the voltage drop rate accelerates significantly. As depicted in Figure 4b, the battery temperature can reach a maximum of 58 °C at an ambient temperature of 45 °C, which has a considerable impact on battery performance. Conversely, at an ambient temperature of 5 °C, the battery temperature is initially low, which is detrimental to discharge performance. However, as the discharge depth increases, the battery temperature rises to a range that is conducive to optimal battery performance.

4.2. Parameter Identification Results

The external physical quantities that can be measured during the battery's charging and discharging process are quite restricted. Typically, these include voltage, circuit, running time, battery temperature, and ambient temperature. However, to develop a comprehensive electric–thermal model of the battery, additional model parameters that describe the internal electrochemical process are necessary. Unfortunately, these parameters cannot be directly measured through experimentation. Consequently, this paper concentrates on identifying model parameters through measured external physical quantities, utilizing Simscape software. The simulation flow chart is illustrated in Figure 5.

Figure 6 displays the electrical parameters R0, R1, and C1 of the battery model in relation to both battery temperature and SOC.

In Figure 6, R0 primarily represents the variation between the battery's electromotive force and the external voltage, taking into account the prevailing environmental temperature and SOC. On the other hand, R1*C1 signifies the duration required for the battery to transition from the current SOC to the subsequent SOC point, considering the current environmental temperature. Here, R1 is the main factor responsible for the external voltage fluctuation observed between the two SOC points. The primary factor contributing to the alterations in the curves depicted in Figure 6b,c could be attributed to non-uniform SOC intervals and significant temperature-related impacts on the parameters.

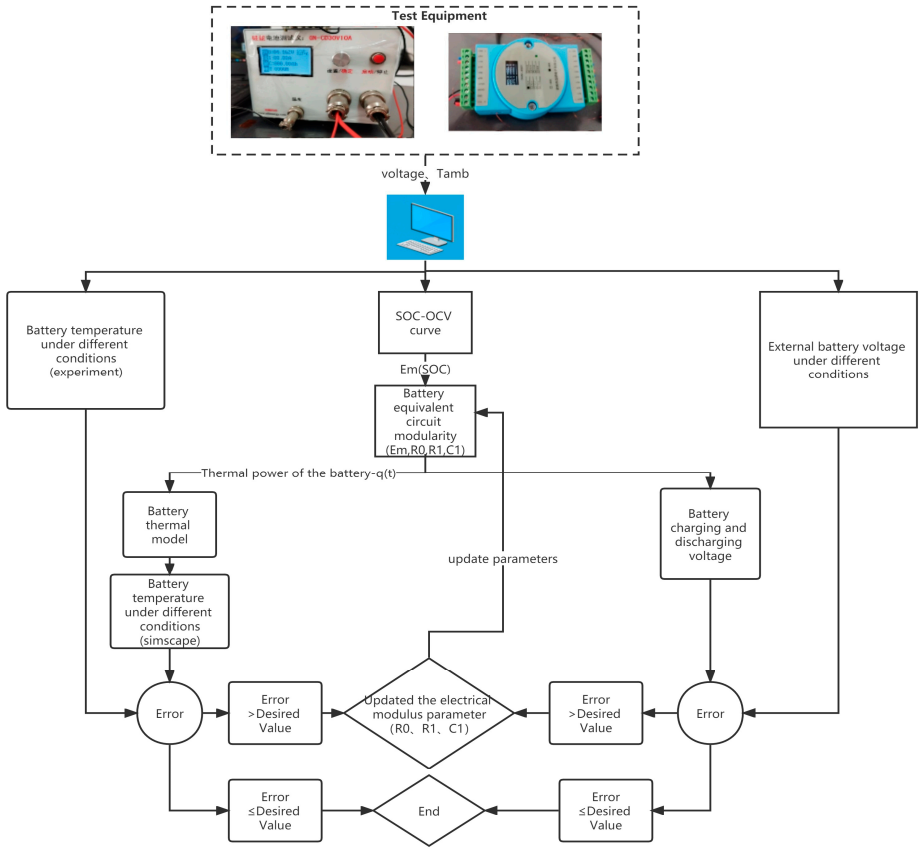

Figure 5. Flowchart for simulation.

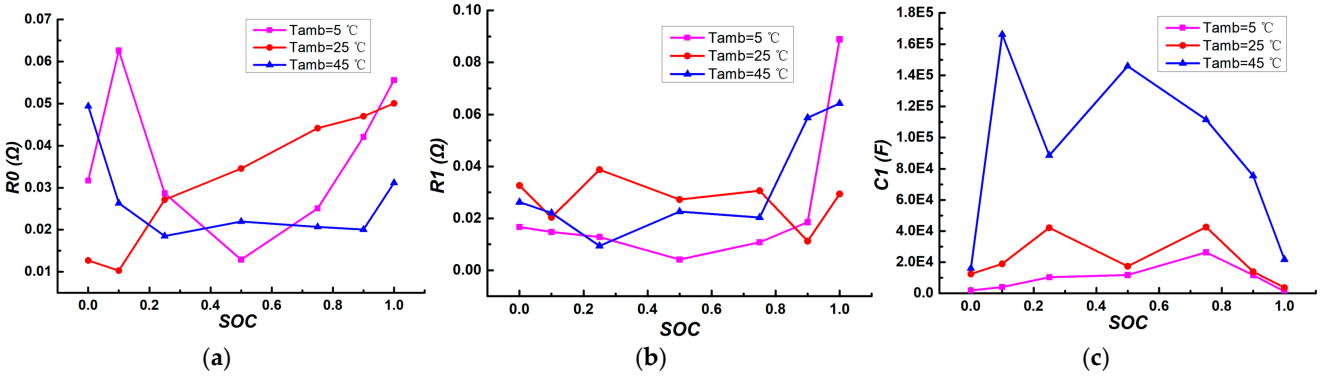

Figure 6. (**a**) Changes of R0 with SOC and ambient temperature; (**b**) Variation of R1 with SOC and ambient temperature; (**c**) Changes of C1 with SOC and ambient temperature.

As depicted in Figure 6a, it is evident that the internal resistance of the battery is high during the initial charging or final discharging stages when the temperature is either low or high. This suggests that the battery's charging and discharging performance can be influenced by both low and high temperatures. At the outset of discharge (SOC = 1), the R0 value is relatively high at different temperatures. This is because, when the battery discharges suddenly, generating an external current, the voltage drops abruptly from the open circuit power supply voltage, resulting in a significant voltage drop. The resistance the battery encounters at the beginning of discharge is greater at lower temperatures, with the maximum R0 occurring at 5 °C. Towards the end of the discharge cycle (when the state of charge is between 0–0.25), the R0 value experiences a significant increase at both low and high temperatures (5 °C and 45 °C). This phenomenon can be mainly attributed to the considerable difference between the external voltage and the battery source's electromotive

force. However, if the battery is operating at an optimal temperature (25 °C), this difference is reduced even further.

In summary, R0 is influenced by multiple factors such as Em(SOC), SOC, and battery temperature, resulting in significant differences in R0 changes at different temperatures. R1 and C1 are determined by the time between adjacent SOC points, variation of external voltage over time during charging and discharging, and temperature. Since the SOC intervals are not uniform in this study and temperature has a significant impact on the external voltage drop, the differences in R1 and C1 at different temperatures will also be significant.

4.3. Model Validation

In this section, a discharge rate of 2C is utilized to verify the model under the same conditions using experimental data measured at varying ambient temperatures. The experiment involved discharging a 21,700 lithium-ion battery at a 2C rate using the CC–CV (constant current–constant voltage) discharge mode, with the battery SOC being discharged from 100% to 0%. The transient terminal voltage and temperature were measured using CN-CD30V10A and a temperature sensor, respectively. The transient terminal voltage and internal temperature of the battery model were recorded under identical conditions. Furthermore, due to the constant discharge mode employed in this study, there exists an almost linear negative correlation between battery SOC and temperature. The relationship between transient terminal voltage and internal temperature with time is opposite to that with SOC. Figure 7 illustrates a comparison of the voltage at the output terminal of the model and the internal temperature of the battery under different temperatures.

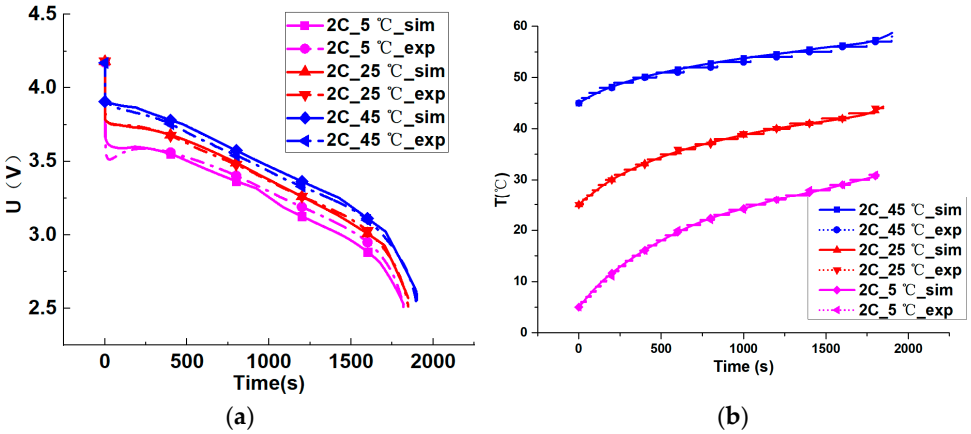

Figure 7. (**a**) Experimental and model output voltages at different ambient temperatures; (**b**) Internal temperature of experimental and model batteries at different ambient temperatures.

Based on Figure 7a, it can be observed that the electric characteristics of the battery model match the actual electric characteristics most accurately at an ambient temperature of 25 °C. However, at an ambient temperature of 5 °C, there is a significant deviation between the electric characteristics of the model and the experimental results during the initial stage of discharge. On the other hand, Figure 7b demonstrates that the thermal characteristics of the model battery align well with the actual battery across different ambient temperatures.

To further investigate the disparity between the simulation and experimental outcomes, this study examines the error between the simulation values and experimental values. Figure 8a displays the relative error between the model transient terminal voltage and the experimental transient terminal voltage over time. Meanwhile, Figure 8b illustrates the absolute error value between the internal temperature of the model and the temperature of the battery pole measured experimentally over time.

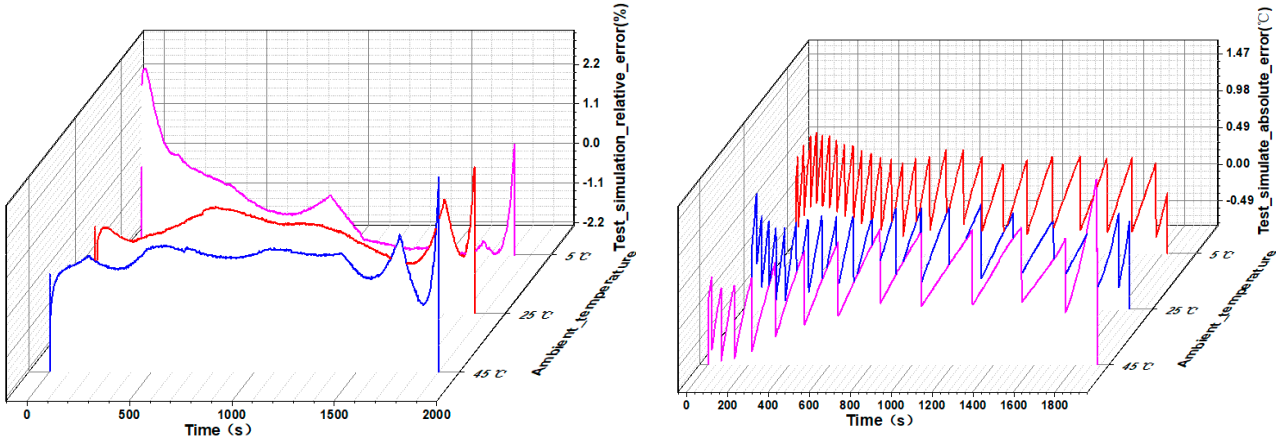

(**a**) (**b**)

Figure 8. (**a**) Relative errors of output voltage between experimental and model at different ambient temperatures; (**b**) Absolute errors of average temperature between experimental and model at different ambient temperatures.

As depicted in Figure 8a, it is evident that the maximum relative error of approximately 2.9% is observed at t = 18 s, when the ambient temperature is 5 °C. However, the relative error experiences a rapid decrease within the first 200 s of discharge time, ultimately dropping to within 0.5% after approximately 156 s. For the majority of the time, the relative error can be maintained within this threshold. However, during the latter stages of discharge, the relative error may increase to some degree. When the ambient temperature is 25 °C or 45 °C, the measured terminal voltage aligns well with the model output transient terminal voltage, with maximum relative errors of approximately 2.85% and 2.89%, respectively.

Based on Figure 8b, it can be observed that, at an ambient temperature of 5 °C, the experiment-simulated internal temperature of the battery has an absolute error of approximately 0.77 °C, occurring at discharge time t = 1518 s. At an ambient temperature of 25 °C, the maximum absolute error is around 0.71 °C, while at 45 °C, the maximum absolute error is significantly larger, at approximately 1.65 °C. These errors are primarily concentrated towards the end of discharge and are of short duration. The absolute error depicted in Figure 8 exhibits a zigzag pattern overall, which is mainly due to the short sampling interval during the experiment. This leads to oscillations in the experimental results along the entire time axis, resulting in a zigzag shape for the absolute error of the experiment-simulation temperature.

Moreover, when compared to the model errors found in other literature, Table 5 illustrates the discrepancies in the models of batteries with varying specifications. It can be inferred that the battery model developed in this study, utilizing the offline parameter identification method, closely approximates the actual performance of the battery. Possible reasons for errors include (1) Battery performance degradation caused by aging is not taken into account; (2) Difficulty in capturing battery dynamic voltage in the low frequency range; and (3) The battery electric–thermal coupling model is based on the assumption that the battery is a uniformly heating body.

Table 5. Comparison of model performance [8].

	Model in This Paper	Model in Lin [8]	Model in Ref	DST	FUDS
Model description	RC&thermal	RC&thermal	RC + hysteresis	RC + hysteresis	RC + hysteresis
Temperature variation (°C)	5~45	25~38	−5~40	Constant	Constant
(Root Mean Square Error) RMSE of Voltage (mV)	49	20.3	26	8	8
RMSE of Ts (°C)	0.31	0.65	—	—	—

5. Numerical Analysis Results of Heat Pipe Heat Management System

Both high and low temperatures can have a significant impact on battery performance. Elevated temperatures can shorten the lifespan of batteries and, in extreme cases, cause thermal runaway. Conversely, low temperatures can lead to the formation of lithium dendrites within the battery, which can negatively affect its charging and discharging capabilities, ultimately reducing its capacity and lifespan. Therefore, it is crucial to cool the battery during high-temperature conditions and heat it during low-temperature conditions to enhance its performance. This article proposes a heat pipe-based thermal management system that can regulate battery temperature within the optimal operating range under both low and high temperature conditions. The advantage of a heat pipe is that when the battery temperature is low and the refrigerant temperature is high, the heat pipe mainly plays the role of heating the battery to improve the performance of the battery. With the increase in discharge depth, when the temperature of the battery is high, the heat pipe plays a cooling effect on the battery to control the working temperature of the battery.

This section primarily focuses on simulating the thermal management effect of a flat heat pipe on batteries. The first part of the study examines the impact of ambient temperature on the thermal management effect. When the battery and ambient temperature are low, the heat pipe's contact end with the battery acts as the condensation end, while the evaporating end couples with the vehicle's air conditioning heating equipment to maintain a temperature of 25 °C. Conversely, when the battery and ambient temperature are high, the contact end of the heat pipe and the battery becomes the evaporating end, and the condensation end couples with the vehicle's air conditioning refrigeration equipment to regulate the cooling liquid's flow rate and maintain the condensation end's temperature at 25 °C.

The second part of the study examines the impact of refrigerant temperature on the thermal management effect. One end of the heat pipe is in contact with the battery, while the other end is cooled or heated through a heat exchanger. When the battery temperature is lower than the refrigerant temperature, the working fluid inside the heat pipe facilitates heat transfer from the heat exchanger end to the battery end through flow and phase change. Conversely, when the battery temperature is higher than the refrigerant temperature, heat is transferred in the same way from the battery end to the heat exchanger end.

5.1. Ambient Temperature Variation Influence

In order to study the thermal management effect of heat pipes on a cell, this section mainly compares the transient temperature of a cell with and without heat pipes. The result is shown in Figure 9.

Figure 9 illustrates the transient temperatures of the battery system with and without heat pipes at varying ambient temperatures (5 °C, 25 °C, 45 °C) and discharge rates (2C). The refrigerant temperature at the contact end of the heat pipe and heat exchanger is maintained at 25 °C. As depicted in the figure, at an ambient temperature of 5 °C, the temperature of the heat pipe system battery increases to 20 °C after discharging for approximately 100 s, and then stabilizes at around 20 °C. Conversely, the temperature of the battery without a heat pipe system remains low during the initial discharge stage, and even after 500 s

of discharge, the temperature is still below 20 °C. As the discharge depth increases, the battery temperature continues to rise and reaches 31 °C at the end of discharge.

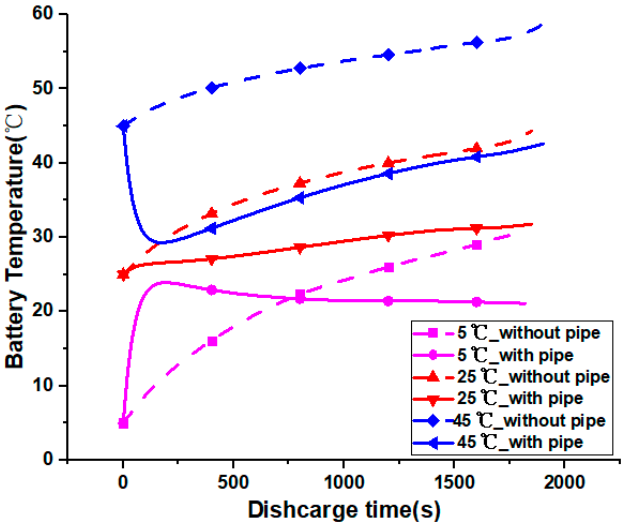

Figure 9. Variation in battery temperature with and without heat pipes with discharge depth at various ambient temperatures.

At an ambient temperature of 25 °C, the transient temperature of the battery system with heat pipes gradually increases and reaches a maximum value of 31.75 °C at the end of discharge. In contrast, the transient temperature of a battery without a heat pipe rises rapidly, reaching 44 °C at the end of discharge.

When the ambient temperature is 45 °C, the initial heat generation rate of the battery system with heat pipes is slow. The heat taken away by the heat pipes is greater than the sum of the heat generated by the battery and the heat exchanged by the environment. Consequently, the transient temperature of the battery drops to approximately 29 °C within 300 s of discharge. However, as the discharge process continues, the heat generated by the battery increases, and the battery temperature rises. The final discharge temperature is 42.59 °C. On the other hand, the transient temperature of the battery without a heat pipe rises faster, reaching 58 °C at the end of discharge.

5.2. Impact of the Refrigerant Temperature

The aim of this section is to examine the impact of the refrigerant temperature at the point of contact between the heat pipe and heat exchanger on the battery's transient temperature. Figure 10 displays the battery's transient temperature under different ambient temperatures of 5 °C, 25 °C, and 45 °C, with corresponding refrigerant temperatures of 15 °C, 18 °C, 20 °C, 22 °C, and 25 °C.

From Figure 10, it is evident that, during the initial stage of discharge, the fluctuation in refrigerant temperature has minimal impact on the battery's transient temperature. However, as the discharge depth increases, the influence becomes more pronounced. At an ambient temperature of 5 °C, all five refrigerant temperatures effectively regulate the battery's thermal performance. After 100 s of discharge, the battery temperature stabilizes at approximately 20 °C, with a rapid initial rise in transient temperature followed by a slight decrease. At an ambient temperature of 25 °C, all 5 refrigerant temperatures result in a similar rate of change in battery temperature during the initial discharge stage, with a large rate of change. As the battery discharge progresses, the rising trend of battery temperature slows down. The terminal discharge temperatures of the battery at refrigerant temperatures of 15 °C, 18 °C, 20 °C, 22 °C, and 25 °C are 29.74 °C, 30.35 °C, 30.76 °C, 31.16 °C, and 31.75 °C, respectively. This implies that for every 3 °C decrease in refrigerant temperature, the terminal temperature of the battery decreases by approximately 0.6 °C. At an ambient

temperature of 45 °C, the transient temperature of the battery exhibits a similar trend at all five refrigerant temperatures. During the initial stage of discharge, the battery temperature drops rapidly, but as the discharge depth increases, the battery temperature reaches an inflection point at around 250 s and then rises. The terminal discharge temperatures of the battery at refrigerant temperatures of 15 °C, 18 °C, 20 °C, 22 °C, and 25 °C are 40.66 °C, 41.24 °C, 41.63 °C, 42.02 °C, and 42.59 °C, respectively. This implies that for every 3 °C decrease in refrigerant temperature, the battery temperature decreases by less than 0.6 °C.

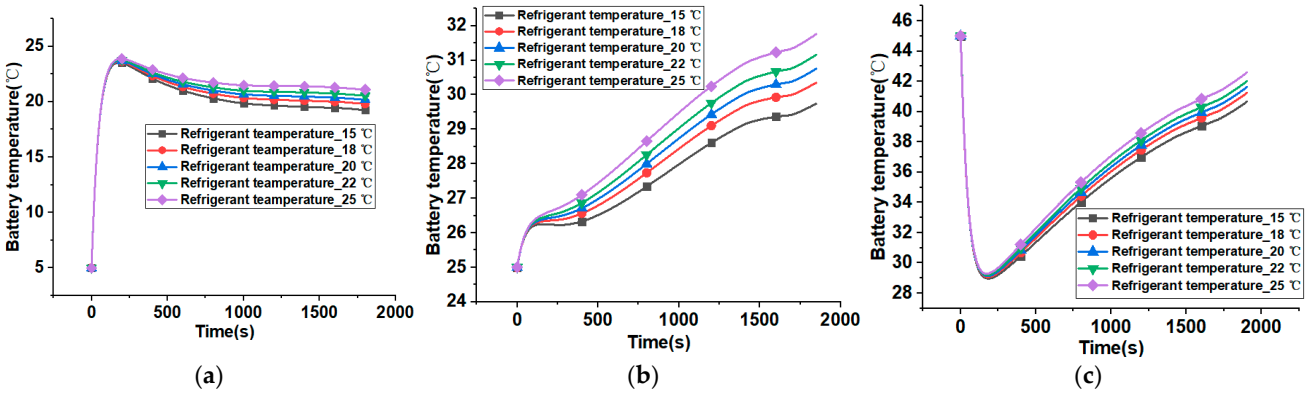

Figure 10. (**a**) Environment temperature_5 °C_Refrigerant temperature impact; (**b**) Environment temperature_25 °C_Refrigerant temperature impact; (**c**) Environment temperature_45 °C_Refrigerant temperature impact.

In summary, the transient temperature of the battery exhibits a similar trend across different refrigerant temperatures. While decreasing the refrigerant temperature can mitigate the transient temperature during battery discharge, the impact is not particularly pronounced. In practical applications, it is important to consider both the energy consumption required to lower the refrigerant temperature and the cooling effect on the battery. This means that both thermal management and cost-effectiveness should be taken into account simultaneously. Specifically, when the ambient temperature is 25 °C, adjusting the refrigerant temperature can yield better thermal management results compared to other temperature conditions.

6. Conclusions

In this paper, a battery electrothermal model coupled with heat pipe flow and heat transfer was established, using a significant amount of experimental data. The study investigated the impact of ambient temperature and refrigerant temperature outside the heat pipe on the transient average temperature of the battery. Based on the findings, it can be concluded as follows:

(1) When the ambient temperature is at 25 °C, the battery parameters exhibit minimal changes during the charging and discharging process, resulting in better battery performance compared to temperatures of 5 °C and 45 °C.

(2) The heat management battery system with heat pipes outperforms the non-heat pipe battery system during battery discharge, effectively controlling battery temperature at both low and high temperatures.

(3) While lowering the refrigerant temperature can reduce the transient temperature during battery discharge, the effect is not significant. In practical applications, the energy consumption required to lower the refrigerant temperature and the battery cooling effect should be considered comprehensively, balancing thermal management effectiveness and economy.

(4) At an ambient temperature of 25 °C, adjusting the refrigerant temperature yields better thermal management results compared to other temperature conditions. Thus,

achieving optimal thermal management requires adjusting the refrigerant temperature under suitable ambient temperature conditions.

In summary, the main innovations of this article are as follows: (1) The feasibility of using a heat pipe for battery thermal management was studied based on a battery electric–thermal coupling model, and effective conclusions were drawn. (2) All studies in this article were transient analyses. (3) Not only the cooling characteristics of the heat pipe on the battery were studied, but also the feasibility of heating the battery with the heat pipe in a low-temperature environment and its impact on battery performance. Based on the research in this article, we will further conduct the following studies: (1) Experimental and simulation studies on the effects of different gravity angles and heat pipe bending angles on thermal management performance. (2) Simulation analysis of the coupling of battery thermal management system and automotive air conditioning.

Author Contributions: Conceptualization, X.H. and Y.Z.; methodology, Y.X.; software, Y.X.; validation, Z.W. and B.L.; formal analysis, Y.X.; investigation, Z.K.; resources, X.H.; data curation, Z.W.; writing—original draft preparation, Y.X.; writing—review and editing, Y.X. All authors have read and agreed to the published version of the manuscript.

Funding: This research was funded by National Regional Science Foundation of China, grant number: 51863014, and by Science and Technology Research Project of Education Department of Jiangxi Province, GJJ191111.

Institutional Review Board Statement: Not applicable.

Informed Consent Statement: Not applicable.

Data Availability Statement: The data supporting the findings of this study can be obtained from the corresponding author upon a reasonable request.

Conflicts of Interest: The authors declare no conflict of interest.

References

1. Hallaj, A.S.; Maleki, H.; Hong, J.S. Thermal modeling and design considerations of lithium-ion batteries. *J. Power Sources* **1999**, *83*, 1–8. [CrossRef]
2. Damay, N.; Forgez, C.; Bichat, M.; Friedrich, G. Thermal modeling of large prismatic $LiFePO_4$/graphite battery. Coupled thermal and heat generation models for characterization and simulation. *J. Power Sources* **2015**, *283*, 37–45. [CrossRef]
3. Andrey, S.; Miroslav, K.; Nalin, C.; Ahmed, J.; Kojic, A. PDE model for thermal dynamics of a large Li-ion battery pack. In Proceedings of the 2011 American Control Conference, San Francisco, CA, USA, 29 June 2011.
4. Hu, Y.; Yurkovich, S. Linear parameter varying battery model identification using subspace methods. *J. Power Sources* **2011**, *196*, 2913–2923. [CrossRef]
5. Chris, M.; Ben, L.; Derrick, B. Advanced Electro-Thermal Modeling of Lithium-Ion Battery System for Hybrid Electric Vehicle Applications. In Proceedings of the Vehicle Power and Propulsion Conference, Arlington, TX, USA, 9–12 September 2007.
6. Shrimali, H.; Patel, P.; Patel, R.; Ray, A.; Mukhopadhyay, I. Electrochemical-thermal modelling of commercially available cylindrical lithium-ion cells for the tropical climate of India. *Mater. Today Proc.* **2021**, *47*, 647–651. [CrossRef]
7. Oehler, F.F.; Nürnberger, K.; Sturm, J.; Jossen, A. Embedded real-time state observer implementation for lithium-ion cells using an electrochemical model and extended Kalman filter. *J. Power Sources* **2022**, *525*, 231018. [CrossRef]
8. Lin, X.; Perez, H.E.; Mohan, S.; Siegel, J.B.; Stefanopoulou, A.G.; Ding, Y.; Castanier, M.P. A lumped-parameter electro-thermal model for cylindrical batteries. *J. Power Sources* **2014**, *257*, 1–11. [CrossRef]
9. Shu, X.; Yang, W.; Guo, Y.; Wei, K.; Qin, B.; Zhu, G. A reliability study of electric vehicle battery from the perspective of power supply system. *J. Power Sources* **2020**, *451*, 227805. [CrossRef]
10. Report of Investigation: Hybrids Plus Plug in Hybrid Electric Vehicle. Available online: https://prius-touring-club.com/librairie/mediatheque/pdf/toyota-prius-a123-car-fire-investigation-report-2008.pdf (accessed on 26 June 2008).
11. Lei, S.; Shi, Y.; Chen, G. A lithium-ion battery-thermal-management design based on phase-change-material thermal storage and spray cooling. *Appl. Therm. Eng.* **2020**, *168*, 114792. [CrossRef]
12. Wang, Q.; Mao, B.; Stoliarov, S.I.; Sun, J. A review of lithium ion battery failure mechanisms and fire prevention strategies. *Prog. Eng. Combust.* **2019**, *73*, 95–131. [CrossRef]
13. Choudhari, V.G.; Dhoble, D.A.S.; Sathe, T.M. A review on effect of heat generation and various thermal management systems for lithium ion battery used for electric vehicle. *J. Energy Storage* **2020**, *32*, 101729. [CrossRef]

14. Chen, J.; Kang, S.; E, J.; Huang, Z.; Wei, K.; Zhang, B.; Zhu, H.; Deng, Y.; Zhang, F.; Liao, G. Effects of different phase change material thermal management strategies on the cooling performance of the power lithium ion batteries: A review. *J. Power Sources* **2019**, *442*, 227228. [CrossRef]
15. Shahjalal, M.; Shams, T.; Islam, M.E.; Alam, W.; Modak, M.; Hossain, S.B.; Ramadesigan, V.; Ahmed, M.R.; Ahmed, H.; Iqbal, A. A review of thermal management for Li-ion batteries: Prospects, challenges, and issues. *J. Energy Storage* **2021**, *39*, 102518. [CrossRef]
16. Jaguemont, J.; Van Mierlo, J. A comprehensive review of future thermal management systems for battery-electrified vehicles. *J. Energy Storage* **2020**, *31*, 101551. [CrossRef]
17. Kim, J.; Oh, J.; Lee, H. Review on battery thermal management system for electric vehicles. *Appl. Therm. Eng.* **2019**, *149*, 192–212. [CrossRef]
18. Panchal, S.; Khasow, R. Numerical modeling and experimental investigation of a prismatic battery subjected to water cooling. *Numer. Heat Transf. Part A Appl.* **2017**, *71*, 626–637. [CrossRef]
19. Park, H. A design of air flow configuration for cooling lithium ion battery in hybrid electric vehicles. *J. Power Sources* **2013**, *239*, 30–36. [CrossRef]
20. Yu, K.; Yang, X.; Cheng, Y.; Li, C. Thermal analysis and two-directional air flow thermal management for lithium-ion battery pack. *J. Power Sources* **2014**, *270*, 193–200. [CrossRef]
21. Fathabadi, H. High thermal performance lithium-ion battery pack including hybrid active–passive thermal management system for using in hybrid/electric vehicles. *Energy* **2014**, *70*, 529–538. [CrossRef]
22. Lin, K.; Gómez-Bombarelli, R. A redox-flow battery with an alloxazine-based organic electrolyte. *Nat. Energy* **2016**, *1*, 16102. [CrossRef]
23. Hakeem, A.; Solyali, D. Empirical thermal performance investigation of a compact lithium ion battery module under forced convection cooling. *Appl. Sci.* **2020**, *10*, 3732. [CrossRef]
24. Mali, V.; Saxena, R.; Kumar, K.; Kalam, A.; Tripathi, B. Review on battery thermal management systems for energy-efficient electric vehicles. *Renew. Sustain. Energy Rev.* **2021**, *151*, 111611. [CrossRef]
25. Li, W.; Peng, X.; Xiao, M. Multi-objective design optimization for mini-channel cooling battery thermal management system in an electric vehicle. *Int. J. Energy Res.* **2019**, *43*, 3668–3680. [CrossRef]
26. Lan, C.; Xu, J.; Qiao, Y.; Ma, Y. Thermal management for high power lithium-ion battery by minichannel aluminum tubes. *Appl. Therm. Eng.* **2016**, *101*, 284–292. [CrossRef]
27. Kairat, I.; Desmond, A. On using splitter plates and flow guide-vanes for battery module cooling. *Heat Mass Transf.* **2017**, *53*, 1–10.
28. Qian, Z.; Li, Y.; Rao, Z. Thermal performance of lithium-ion battery thermal management system by using mini-channel cooling. *Energy Convers. Manag.* **2016**, *126*, 622–631. [CrossRef]
29. Najjar, A.; Hussein, M.T.; Jasim, M.M.; Dmitry, O.B.; Nidhal, B.K.; Naif, K.A.; Maria, J.O.; Moram, A.F.; Wahiba, Y.; Pouyan, T.M. Improving the Melting Duration of a PV/PCM System Integrated with Different Metal Foam Configurations for Thermal Energy Management. *Nanomaterials* **2022**, *12*, 423. [CrossRef]
30. Nidhal, B.K.; Rashad, A.B.; Lioua, K.; Mohamed, O. Performance investigation of a vertically configured LHTES via the combination of nano-enhanced PCM and fins: Experimental and numerical approaches. *Int. Commun. Heat Mass Transf.* **2022**, *137*, 106246.
31. Wilke, S.; Schweitzer, B.; Khateeb, S.; Al-Hallaj, S. Preventing thermal runaway propagation in lithium ion battery packs using a phase change composite material: An experimental study. *J. Power Sources* **2017**, *340*, 51–59. [CrossRef]
32. Qiu, F.; Li, X.; Deng, H.; Wang, D.; Mu, X.; He, P.; Zhou, H. A Concentrated Ternary-Salts Electrolyte for High Reversible Li Metal Battery with Slight Excess Li. *Adv. Energy Mater.* **2019**, *9*, 1803372. [CrossRef]
33. Heyhat, M.M.; Mousavi, S.; Siavashi, M. Battery thermal management with thermal energy storage composites of PCM, metal foam, fin and nanoparticle. *J. Energy Storage* **2020**, *28*, 101235. [CrossRef]
34. Jilte, R.; Afzal, A.; Panchal, S. A novel battery thermal management system using nano-enhanced phase change materials. *Energy* **2021**, *219*, 119564. [CrossRef]
35. Aslam, S.; Sagar, R.U.R.; Liu, Y.; Anwar, T.; Zhang, L.; Zhang, M.; Mahmood, N.; Qiu, Y. Graphene decorated polymeric flexible materials for lightweight high areal energy lithium-ion batteries. *Appl. Mater. Today* **2019**, *17*, 123–129. [CrossRef]
36. Nidhal, B.K.; Fatih, S.; Lioua, K. Performance Optimization of a Thermoelectric Device by Using a Shear Thinning Nanofluid and Rotating Cylinder in a Cavity with Ventilation Ports. *Mathematics* **2022**, *10*, 1075.
37. Lyu, Y.; Siddique, A.R.M.; Majid, S.H.; Biglarbegian, M.; Gadsden, S.A.; Mahmud, S. Electric vehicle battery thermal management system with thermoelectric cooling. *Energy Rep.* **2019**, *5*, 822–827. [CrossRef]
38. Lyu, Y.; Siddique, A.R.M.; Gadsden, S.A.; Mahmud, S. Experimental investigation of thermoelectric cooling for a new battery pack design in a copper holder. *Results Eng.* **2021**, *10*, 100214. [CrossRef]
39. Liao, G.; Jiang, K.; Zhang, F.; Liu, L.; Chen, J.; Leng, E. Thermal performance of battery thermal management system coupled with phase change material and thermoelectric elements. *J. Energy Storage* **2021**, *43*, 103217. [CrossRef]
40. Liang, J.; Gan, Y.; Li, Y. Investigation on the thermal performance of a battery thermal management system using heat pipe under different ambient temperatures. *Energy Convers. Manag.* **2018**, *155*, 1–9. [CrossRef]
41. Yuan, W.; Yan, Z.; Chen, W. Heat-pipe-based thermal management and temperature characteristics of Li-ion batteries. *Can. J. Chem. Eng.* **2016**, *94*, 1901–1908. [CrossRef]

42. Kalbasi, R. Introducing a novel heat sink comprising PCM and air—Adapted to electronic device thermal management. *Int. J. Heat Mass Transf.* **2021**, *169*, 120914. [CrossRef]
43. Zhao, J.; Lv, P.; Rao, Z. Experimental study on the thermal management performance of phase change material coupled with heat pipe for cylindrical power battery pack. *Exp. Therm. Fluid Sci.* **2017**, *82*, 182–188. [CrossRef]
44. Yamada, T.; Koshiyama, T.; Yoshikawa, M. Analysis of a lithiumion battery cooling system for electric vehicles using a phase-change material and heat pipes. *J. Therm. Sci.* **2017**, *12*, JTST0011. [CrossRef]
45. Tran, T.; Harmand, S.; Desmet, B.; Filangi, S. Experimental investigation on the feasibility of heat pipe cooling for HEV/EV lithium-ion battery. *Appl. Therm. Eng.* **2014**, *63*, 551–558. [CrossRef]
46. Wang, Q.; Jiang, B.; Xue, Q.F.; Sun, H.L.; Li, B.; Zou, H.M.; Yan, Y.Y. Experimental investigation on EV battery cooling and heating by heat pipes. *Appl. Therm. Eng.* **2015**, *88*, 54–60. [CrossRef]
47. Alihosseini, A.; Shafaee, M. Experimental study and numerical simulation of a Lithium-ion battery thermal management system using a heat pipe. *J. Energy Storage* **2021**, *39*, 102616. [CrossRef]
48. Tran, T.; Harmand, S.; Sahut, B. Experimental investigation on heat pipe cooling for Hybrid Electric Vehicle and Electric Vehicle lithium-ion battery. *J. Power Sources* **2014**, *265*, 262–272. [CrossRef]